

ALICE-INT-2012-xxx
November 28, 2012

2

3

4

**Two-proton correlations in Pb–Pb collisions at $\sqrt{s_{NN}} = 2.76$ TeV
from the ALICE experiment at the LHC**

5

Maciej Szymański¹
Adam Kisiel¹

6

1. Warsaw University of Technology

7

Email: Maciej.Szymanski@cern.ch
Adam.Kisiel@cern.ch

8

Abstract

9

10

11

12

13

14

15

16

Correlations of all combinations of pairs of protons and antiprotons are measured in Pb–Pb collisions at $\sqrt{s_{NN}} = 2.76$ TeV in the ALICE experiment. One-dimensional pp , $\bar{p}\bar{p}$ and $p\bar{p}$ correlation functions are formed in three centrality and two pair transverse momentum ranges. The femtoscopic parameters for the radius of the proton source are extracted. The fit includes final-state interactions (strong and Coulomb) and quantum statistics, in case of identical pairs of (anti)protons. Also, the fit takes into account residual correlations coming from $p\Lambda$ system. Two-proton correlations show an increase of the radius with increasing multiplicity and slight decrease of the radius with increasing pair transverse momentum.

| | | |
|----|---------------------------------------|-----------|
| 17 | Contents | |
| 18 | 1 Introduction | 2 |
| 19 | 2 Data analysis | 2 |
| 20 | 2.1 Data sample | 2 |
| 21 | 2.1.1 Collision data | 2 |
| 22 | 2.1.2 Monte Carlo | 2 |
| 23 | 2.2 Analysis software | 2 |
| 24 | 2.3 Event selection | 3 |
| 25 | 2.4 Particle identification | 3 |
| 26 | 2.5 Track selection | 4 |
| 27 | 2.6 Pair selection | 5 |
| 28 | 2.7 Correlation functions | 5 |
| 29 | 3 Results | 6 |
| 30 | 4 Summary | 17 |

1 Introduction

In the analysis, we present the measurements of two-proton correlations in Pb–Pb collisions at $\sqrt{s_{NN}} = 2.76$ TeV registered by the ALICE experiment. The method of two-particle correlations (commonly referred to as *femtoscopy*) allows for extracting the space-time characteristics of the emitting source created in heavy-ion collision. Correlations of identical bosons have been usually used to perform this study. In particular, the ALICE Collaboration has recently carried out the analysis of two-pion correlations in central Pb–Pb collisions [1]. Proton-proton correlations have also been measured for the broad range of the energies of heavy-ion collisions, especially in Au+Au collisions at $\sqrt{s_{NN}} = 200$ GeV by the STAR experiment at RHIC [2].

The main motivation to carry out two-proton femtoscopic study is to complement information about the source size deduced from the correlations of pions and kaons. The analysis provides a test of the hydrodynamic prediction of the transverse mass scaling and gives a possibility for checking if the collectivity also includes baryons. Due to the fact that feed-down from weak decays cannot be neglected in high-energy heavy-ion collisions, the effects of residual correlations related with the p Λ system should be taken into account in the study of proton femtoscopy. Because of the low decay momentum of Λ decay into p and π^- with respect to the mass of proton, femtoscopic correlations between a Λ and a primary proton might still be detected for a pair consisting of a primary proton and the proton from Λ . Furthermore, proton-antiproton correlations should be investigated as a proof that the influence of final-state interaction (the annihilation) may contribute to lowering multiplicities of protons observed at LHC energies, with respect to predictions from chemical models.

2 Data analysis

2.1 Data sample

2.1.1 Collision data

The data used in this note come from Pb–Pb collisions recorded by the ALICE experiment during the 2011 run at the LHC (production LHC11h, pass 2). Analysis Object Data (AOD095) files have been used in studies. About 35 million events have been analysed. The following runs have been used (flagged as 1 (good runs) in RCT):

170593, 170572, 170388, 170387, 170315, 170313, 170312, 170311, 170309, 170308, 170306, 170270, 170269, 170268, 170230, 170228, 170207, 170204, 170203, 170193, 170163, 170159, 170155, 170091, 170089, 170088, 170085, 170084, 170083, 170081, 170040, 170027, 169965, 169923, 169859, 169858, 169855, 169846, 169838, 169837, 169835, 169591, 169588, 169586, 169557, 169554, 169550, 169512, 169504, 169498, 169475, 169419, 169418, 169417, 169415, 169411, 169238, 169167, 169160, 169156, 169148, 169145, 169144, 169138, 169099, 169094, 169091, 169044, 169035, 168992, 168988, 168826, 168777, 168514, 168512, 168511, 168467, 168464, 168460, 168458, 168362, 168361, 168342, 168341, 168325, 168322, 168311, 168310, 168115, 168108, 168107, 168105, 168076, 168069, 167988, 167987, 167985, 167920, 167915

The analysis was done as a part of the “Lego Trains” (run 129 with LHC11h_AOD095).

2.1.2 Monte Carlo

We used the HIJING production LHC11a10a_bis and AMPT production LHC12a11a AOD081.

2.2 Analysis software

The analysis was performed using the AliFemto package being a part of AliROOT framework (v5-03-34-AN):

73 <http://alisoft.cern.ch/viewvc/tags/v5-03-34-AN/PWGCF/FEMTOSCOPY/>.

74 Measured correlation functions have been fitted with the custom written software. It required the input
 75 from THERMINATOR model [3], which is a particle and event generator basing on Monte Carlo methods.
 76 The model aims to study particle production in relativistic heavy ion collisions at the energies available
 77 at RHIC and LHC. THERMINATOR uses the statistical approach to describe particle production. Also, the
 78 chemical and kinetic freeze-out are assumed to occur simultaneously (*single freeze-out model*).

79 The fitting program makes also use of theoretical pp and pA correlation functions. The former one is cal-
 80 culated with CorrFit software [4], which compares the measured correlation function and a model one
 81 calculated using Lednický's weights, experimental distribution of particles' momenta and an assumed
 82 emission source distribution via χ^2 test in the given range of fitting parameters. The latter one is ob-
 83 tained from the analytical formula of Lednický [5], which uses the parametrization of strong interaction
 84 for pA system. The correlation function is calculated as the square of the wave function averaged over the
 85 total spin and over the assumed gaussian distribution of the relative distance between particle emission
 86 points in the pair rest frame.

87 2.3 Event selection

88 Events for the analysis were selected using minimum bias (kMB), central (kCentral) and semicentral
 89 (kSemiCentral) triggers. Events were required to have the collision vertex position within ± 8 cm from
 90 the centre of TPC, measured along the beam axis. The centrality selection classes are used to determine
 91 the centrality with the V0.

92 2.4 Particle identification

93 The analysis of pion femtoscopy in Pb–Pb collisions has shown that there is a need to use the so-called
 94 *TPC-only tracks* constrained to the SPD vertex (with AOD filter bit 7 set). The main reason for this is
 95 related to the fact that global tracking forces some pairs of tracks to have very similar momenta that leads
 96 to distortions in the shape of correlation functions for the lowest values of the momentum difference and,
 97 as a consequence, incorrect extracted source radii [6]. It has also been shown that the *number of σ 's*
 98 method gives more pure sample of particles than the Bayesian PID method [8]. However, *TPC-only*
 99 *tracks* in the AOD data files have only Bayesian PID and there is not enough information to use the $n\sigma$
 100 method (e.g. TPC and TOF signals are missing). The solution of the above problem [7] is as follows: in
 101 AOD files, each *TPC-only track* has its equivalent amongst *global tracks* (having very similar parameters)
 102 related by:

103 `tpcOnlyTrack->GetID() = - 1 - globalTrack->GetID() .`

104 Hence, there is a need to loop over all *global tracks* to save their indices and IDs. Afterwards, in a loop
 105 over *TPC-only tracks*, one is able to get directly a *global track* which corresponds to the current *TPC-*
 106 *only track* and copy the PID information. This procedure was implemented as a part of the AliFemto
 107 package. Femtoscopy analysis requires as pure sample of particles as possible but also high statistics of
 108 them. A combined TPC and TOF method was applied to select (anti)protons. The details of the cut are
 109 as follows:

- 110 – 3σ cut from TPC for tracks with TOF signal and for tracks without TOF signal for momenta less
 111 than $0.5 \text{ GeV}/c$
- 112 – 2σ cut from TPC for momenta in range $(0.5, 0.8) \text{ GeV}/c$ for tracks without TOF signal
- 113 – maximum momentum for tracks only with TPC signal set to $0.8 \text{ GeV}/c$

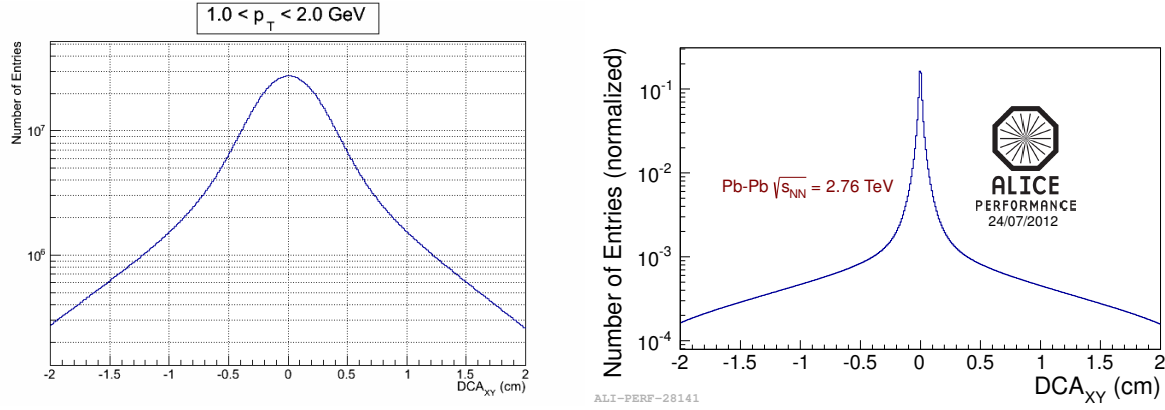


Fig. 1: The comparison of the DCA distribution in the transverse plane for *TPC-only tracks* (left panel) and *global tracks* (right panel).

– 3σ cut from TOF for momenta less than 1.5 GeV/c

– 2σ cut from TOF for momenta higher than 1.5 GeV/c

Additionally, the proton identification was adjusted with the “contour” method. Due to contamination in the proton sample in momentum range 0.5-0.8 GeV/c after $n\sigma$ cut, the track passes PID selection only if its dE/dx value for a given momentum is inside the contour composed of straight lines which parameters were evaluated experimentally to reduce misidentification.

PID purity estimated with MC simulations (AMPT and HIJING) is not less than 99%.

2.5 Track selection

Tracks within the pseudorapidity range $|\eta| < 0.8$ have been selected. To reduce contamination from material, we have chosen protons with $p_T > 0.5$ GeV/c. For antiprotons, there are no explicit constraints on the transverse momentum. We only have limits from PID. Furthermore, the cut on a Distance of Closest Approach (DCA) was applied. Particles located within 0.1 cm in the transverse plane and 2.0 cm in the beam direction with respect to the primary vertex, were accepted. To calculate DCA values, we used `PropagateToDCA` method. It is applied for the *global tracks* corresponding to *TPC-only tracks* (similarly as with PID) because of better resolution. The comparison of the DCA distribution in the transverse plane for *TPC-only tracks* and *global tracks* is shown in Fig. 1. The cut value 0.1 cm was determined using MC simulations to obtain the highest significance. Purity of (anti)protons estimated in MC (HIJING and AMPT) simulations is shown in Tab. 1. The DCA distribution of protons with respect to its origin from MC simulation (AMPT) is shown in Fig. 2.

| | HIJING | | AMPT | |
|-------------|--------|-----------|------|-----------|
| | p | \bar{p} | p | \bar{p} |
| primary | 91% | 90% | 88% | 80% |
| weak decays | 8% | 9% | 11% | 20% |
| material | 1% | 1% | 1% | 0% |

Table 1: Fractions of (anti)protons with respect to its origin from MC simulations.

The minimum number of TPC clusters corresponding to the given track was set to 80 (out of all 159 clusters). The maximum value of χ^2 per TPC cluster was 4.0 (2 degrees of freedom per cluster).

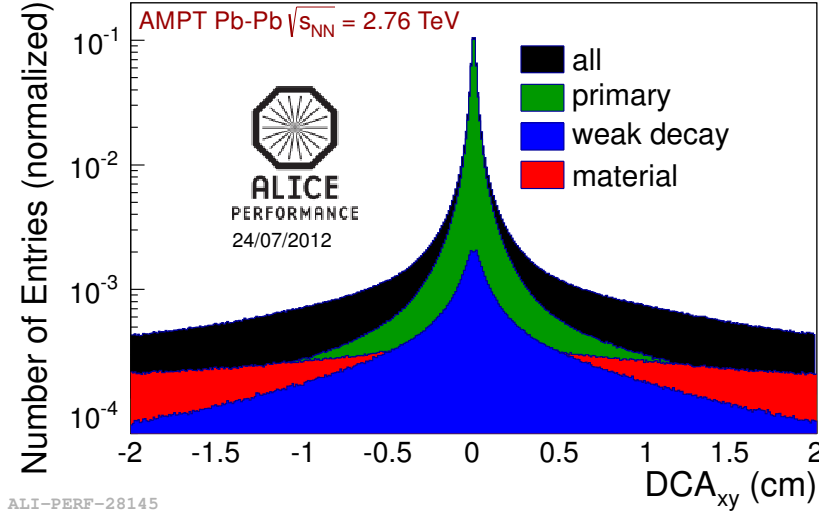


Fig. 2: The DCA distribution of protons with respect to its origin from MC simulation (AMPT).

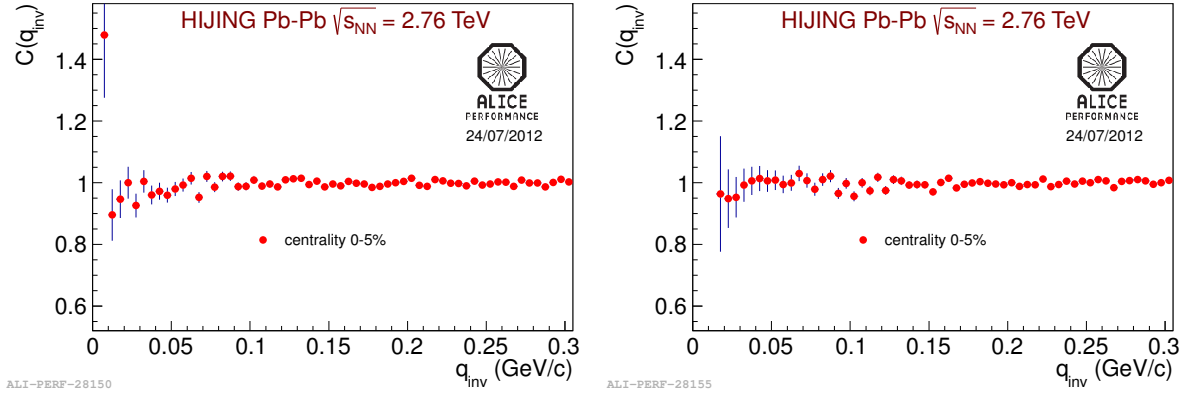


Fig. 3: pp correlation function from HIJING simulations without the cut on angular distance (left panel) and with the cut $|\Delta\phi^*| < 0.02$, $|\Delta\eta| < 0.015$ (right panel).

2.6 Pair selection

In case of pair selection criteria, standard cuts preventing the effects of merging (two tracks reconstructed as one) and splitting (one track reconstructed as two) were used. Strictly speaking, the cuts consists of two steps: *share quality* and *share fraction*. The former one bases on the calculation of the fraction of the number of clusters on the same TPC pad row shared by both tracks to the number of all clusters of the two tracks. Maximum *share quality* was set to 1.0 which means accepting all pairs. As regards *share fraction*, it is obtained as a ratio of shared clusters to all clusters of both tracks. All pairs sharing more than 5% clusters were rejected.

Due to merging effects seen in correlation functions calculated from HIJING simulations (Fig. 3), the cut on angular distance [9] was applied $|\Delta\phi^*| < 0.012$, $|\Delta\eta| < 0.015$). In Fig.4 $\Delta\phi^*\Delta\eta$ distribution from HIJING simulations is shown. Due to the necessity of the knowledge of magnetic field polarity, the analysis need to be performed for *field --* and *field ++* runs separately. However, obtained correlation functions are consistent, so we use all runs together, to have bigger statistics.

2.7 Correlation functions

Two-particle correlations were studied in one dimensional representation with respect to the relative momentum $q_{\text{inv}} = 2 \cdot k^* = \sqrt{(p_1 - p_2)^2 - (E_1 - E_2)^2}$. The correlation effect was measured with the

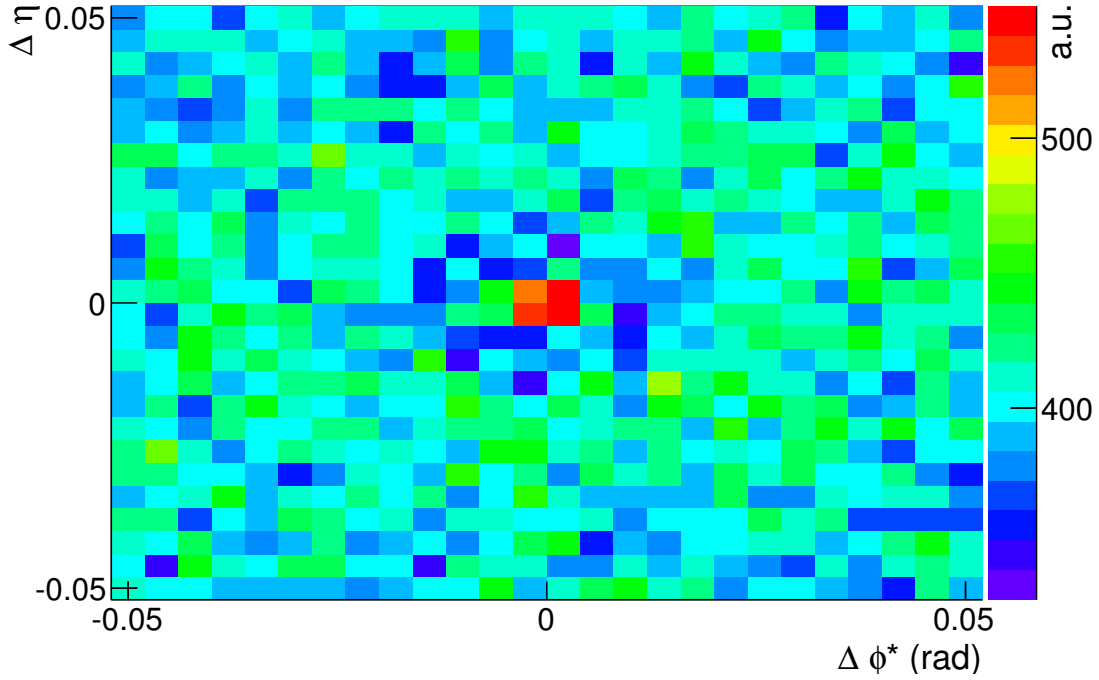


Fig. 4: $\Delta\phi^*\Delta\eta$ distribution from HIJING simulations.

function defined as:

$$C(q_{\text{inv}}) = \frac{A(q_{\text{inv}})}{B(q_{\text{inv}})}, \quad (1)$$

where $A(q_{\text{inv}})$ is a distribution of correlated pairs of particles (coming from the same event), $B(q_{\text{inv}})$ is a distribution of uncorrelated pairs of particles (coming from different events - 10 events were used to create the background distribution).

The analysis has been performed for six centrality bins (0 – 5%, 5 – 10%, 10 – 20%, 20 – 30%, 30 – 40%, 40 – 50%) and then merged into three classes: 0 – 10%, 10 – 30% and 30 – 50%. Also, correlation functions have been calculated for two bins of the pair transverse momentum $k_T = (|\vec{p}_{T,1} + \vec{p}_{T,2}|)/2$: $0.3 < k_T < 1.0$ GeV/c and $k_T > 1.0$ GeV/c. Results for pp pairs were asked to approve only for the second bin of k_T (due to not clear strong correlation for lowest values of q_{inv} seen for the first bin, possibly caused by protons from material, see Fig. 5). Results for $\bar{p}\bar{p}$ are shown for the merged two k_T bins and for the second bin, whereas for $p\bar{p}$: only for the merged two k_T bins.

3 Results

In Fig. 6, 7, 8 and 9 the correlation functions of pp, $\bar{p}\bar{p}$ and $p\bar{p}$ systems are presented. In case of identical systems, the expected maximum due to strong interactions for $q_{\text{inv}} \approx 40$ MeV/c is clearly visible. The results reveal that proton-proton and antiproton-antiproton correlations are consistent. Also, the centrality dependence is understandable - the more peripheral the events, the stronger the correlation effect is. It means that the size of the emitting source is growing with multiplicity. Proton-antiproton correlations show expected behaviour - a maximum for the lowest momentum difference due to Coulomb attraction, then a minimum caused by the annihilation processes. Another observed feature is the flat background of the correlation function at large values of momentum difference which indicates the absence of wide non-femtoscopic structures.

In Fig. 10 the correlation functions are compared with those calculated without the cut on angular dis-

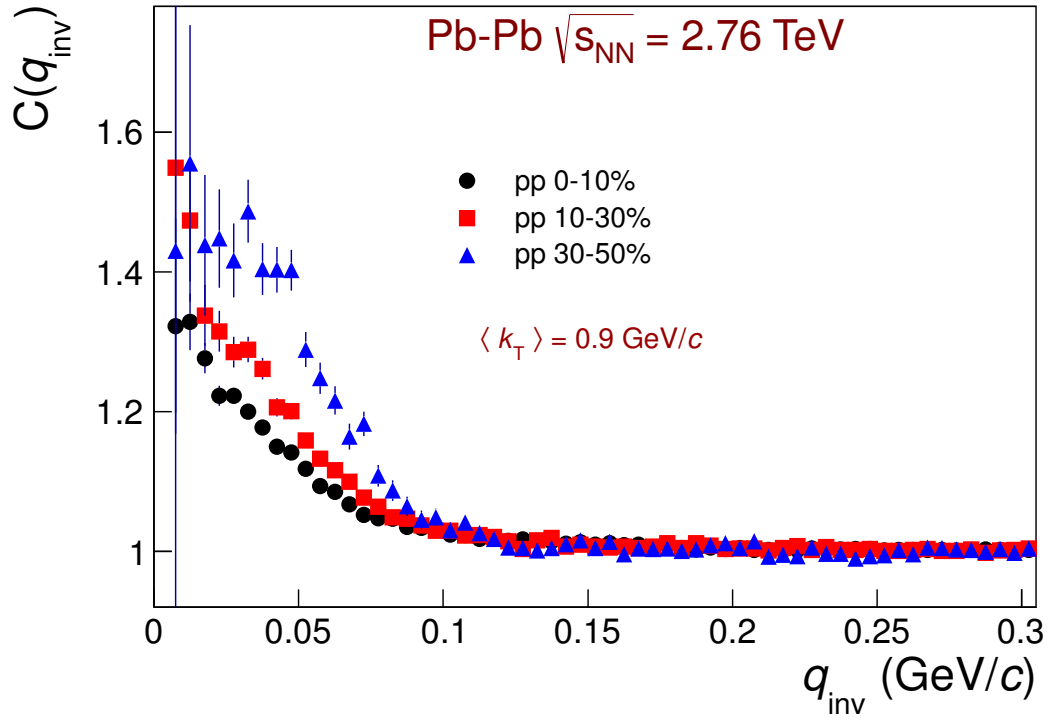


Fig. 5: Proton-proton correlation functions for the $\sqrt{s_{\text{NN}}} = 2.76 \text{ TeV}$ Pb–Pb collision data.

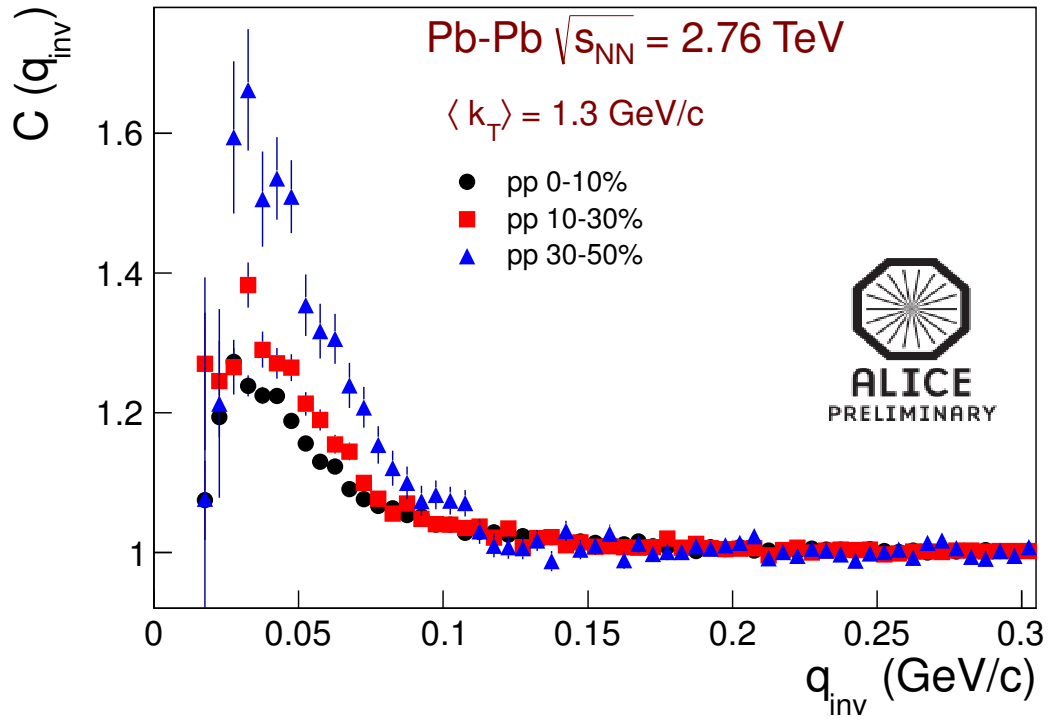


Fig. 6: Proton-proton correlation functions for the $\sqrt{s_{\text{NN}}} = 2.76 \text{ TeV}$ Pb–Pb collision data.

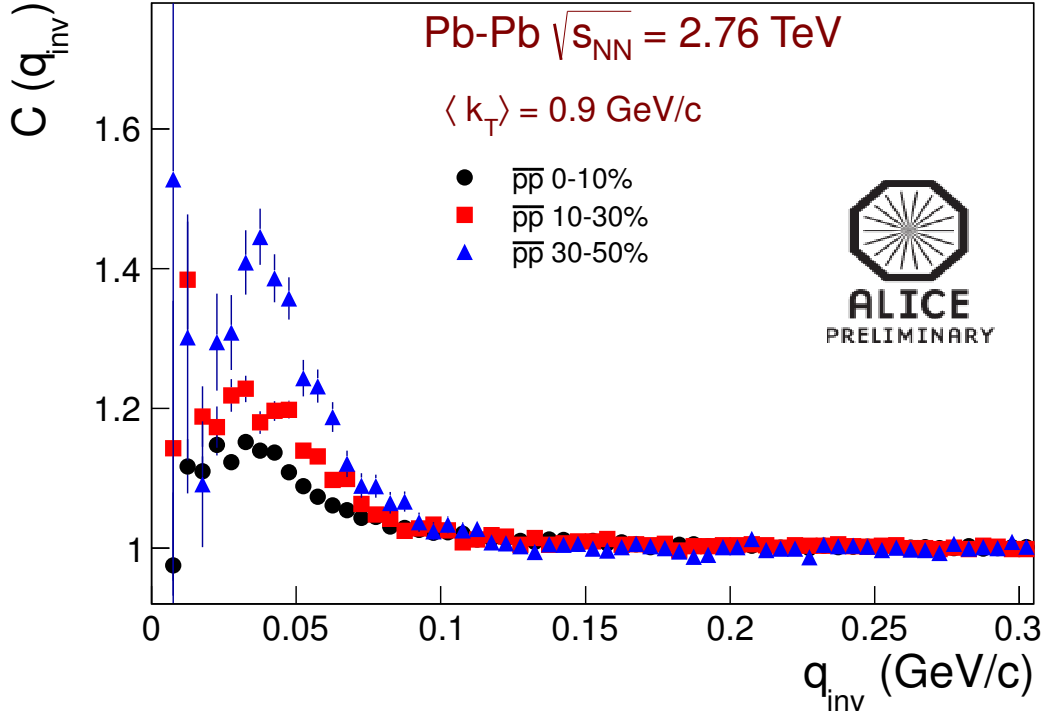


Fig. 7: Antiproton-antiproton correlation functions for the $\sqrt{s_{NN}} = 2.76$ TeV Pb-Pb collision data ($\langle k_T \rangle = 0.9$ GeV/c).

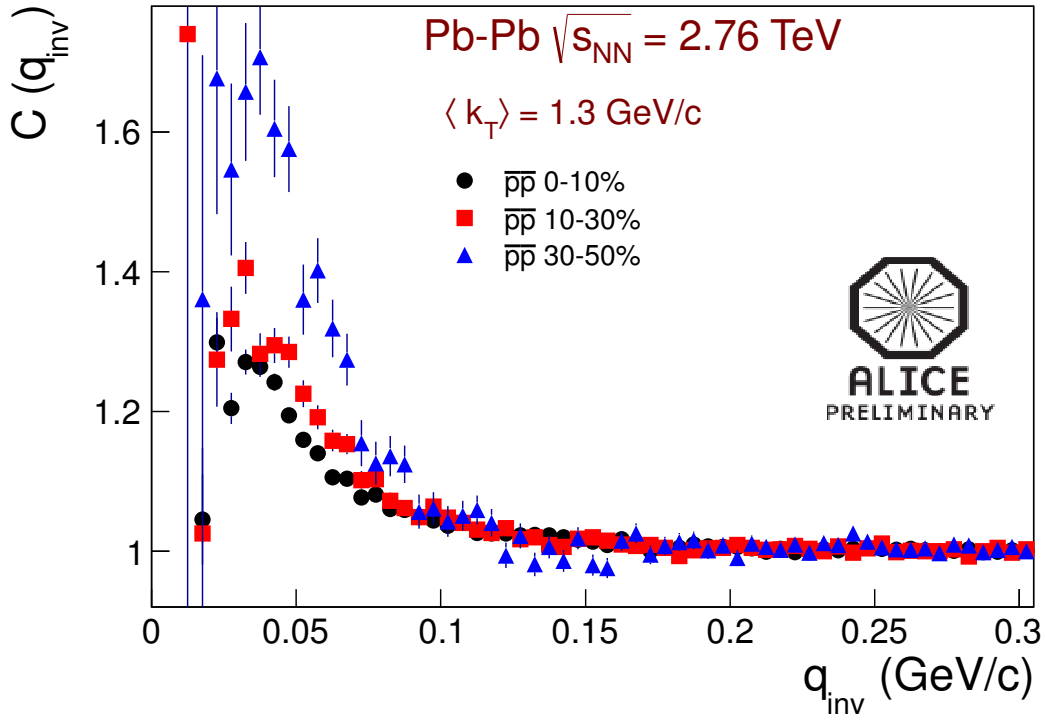


Fig. 8: Antiproton-antiproton correlation functions for the $\sqrt{s_{NN}} = 2.76$ TeV Pb-Pb collision data ($\langle k_T \rangle = 1.3$ GeV/c).

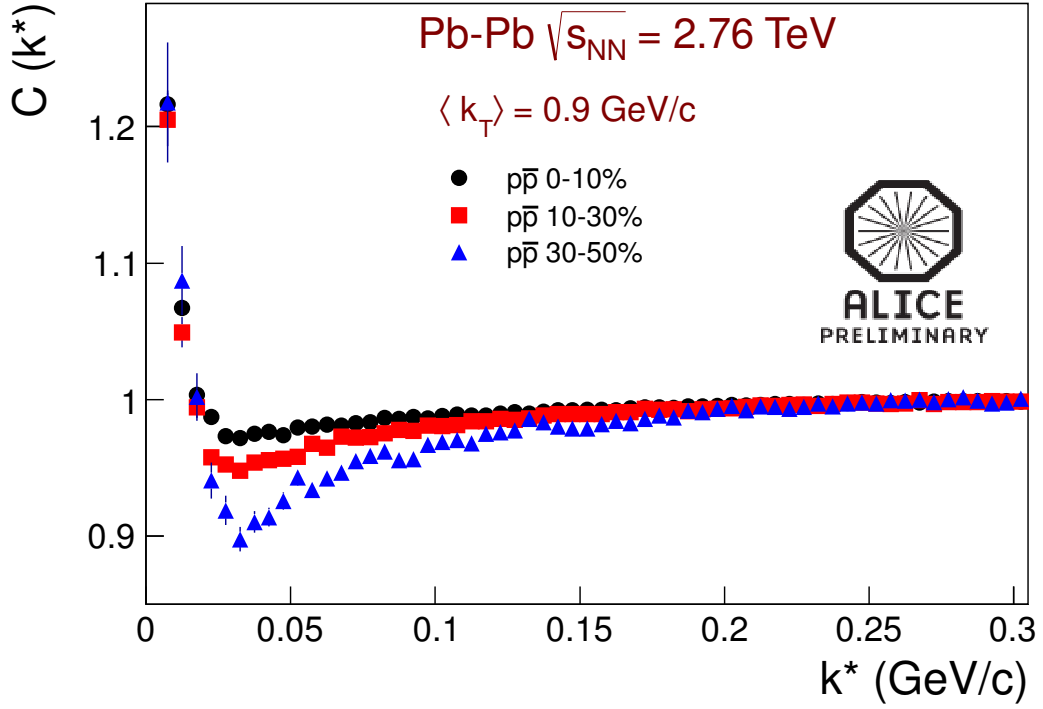


Fig. 9: Proton-antiproton correlation functions for the $\sqrt{s_{NN}} = 2.76$ TeV Pb–Pb collision data.

173 tance. Differences in correlation functions are within statistical errors.

174 In Fig. 11 the comparison of correlation functions calculated for “field —” and “field ++” runs is
 175 shown. The only visible difference can be noticed for proton-antiproton correlation function (centrality
 176 0 – 10%). However, radii fitted for these functions are within statistical and systematic errors shown
 177 below.

Fitting the correlation functions for proton systems can be performed with the software package `CorrFit`. However, as it can be seen in Fig. 12, attempts to fit the obtained correlation functions directly with `CorrFit` failed. Correlation of pp pairs has three components. The Coulomb and quantum statistics have to be negative (e.g. give the correlation function below unity). The strong interaction is positive but has limited width - one can think of it as a resonance peak. Therefore, the excess in the range 30 – 80 MeV/c of k^* cannot be explained by correlations coming from the pp wave function. A significant influence of residual correlations may be a possible explanation. As the influence of residual correlations seems to be significant, the method of simultaneous fitting of pp ($\bar{p}\bar{p}$) and p Λ ($\bar{p}\bar{\Lambda}$) correlations was proposed. It is assumed that residual correlations coming from p Σ^+ system are negligible, due to a known small cross-section for this system. Hence, the experimental correlation function of pp and $\bar{p}\bar{p}$ systems were fitted with the formula:

$$C_{\text{meas}}(k_{pp}^*) = 1 + \lambda_{pp} \cdot (C_{pp}(k_{pp}^*; R) - 1) + \lambda_{p\Lambda} \cdot (C_{p\Lambda}(k_{pp}^*; R) - 1), \quad (2)$$

178 where:

- 179 – λ_{pp} , $\lambda_{p\Lambda}$ - parameters which describes the relative number of pp pairs where both particles are
 180 primary (λ_{pp}) and pairs where one particle is primary, the other is a product of Λ decay ($\lambda_{p\Lambda}$),
- 181 – R - radius
- 182 – $C_{pp}(k_{pp}^*; R)$ - theoretical proton-proton correlation function for given R (Gaussian source assumed),
 183 obtained from `CorrFit`,

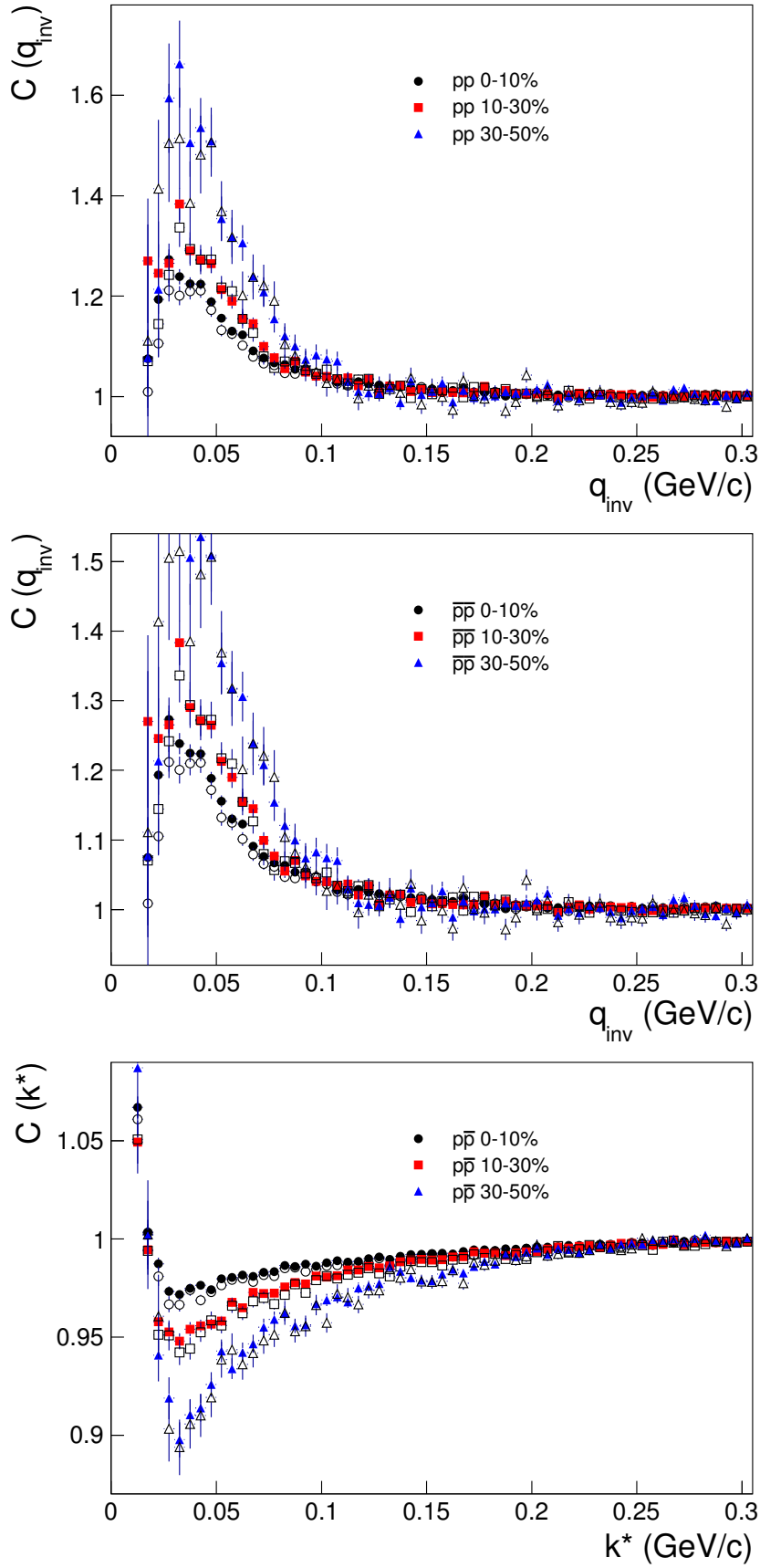


Fig. 10: From top to bottom: proton-proton, antiproton-antiproton and proton-antiproton correlation functions. Results before (open markers) and after (solid markers) applying the cut on angular distance are shown.

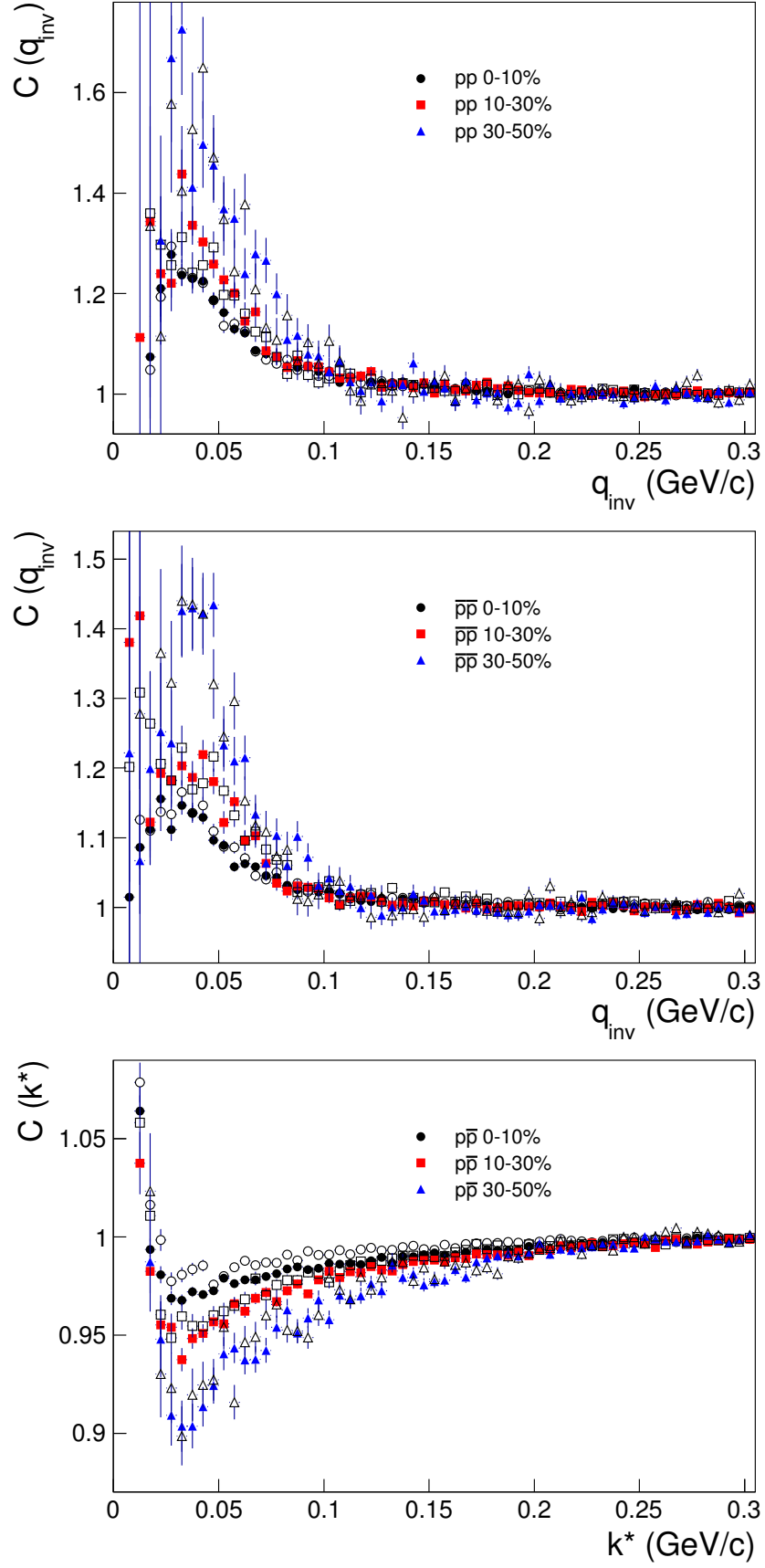


Fig. 11: From top to bottom: proton-proton, antiproton-antiproton and proton-antiproton correlation functions. Results for “field ++” runs (open markers) and “field --” runs (solid markers) are shown.

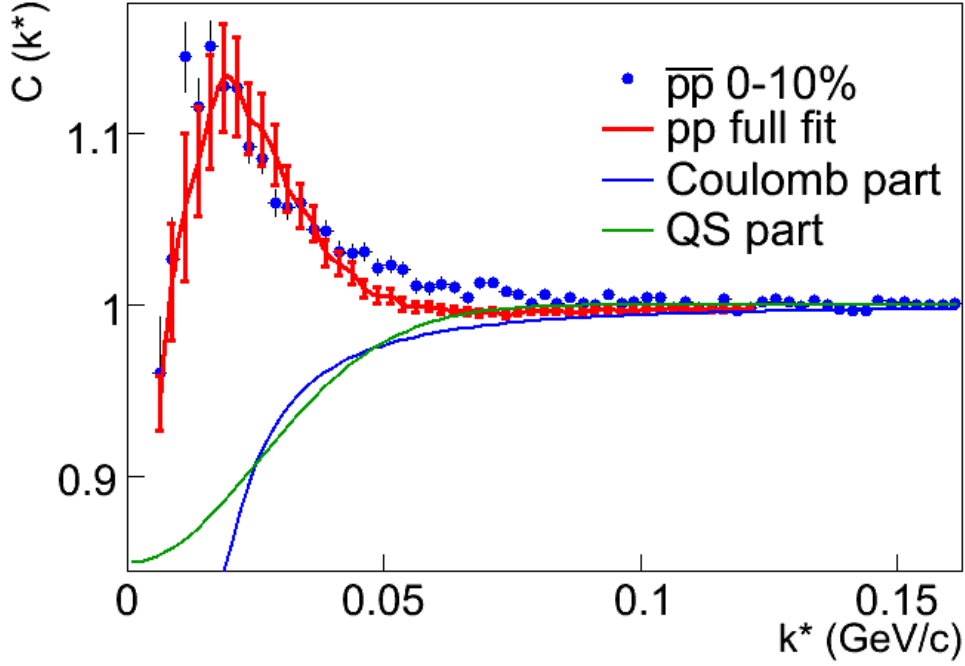


Fig. 12: Comparison of experimental correlation functions and fit obtained with CorrFit [4]. Contribution of Coulomb repulsion and Quantum Statistics are also shown [5].

- 184 – $C_{p\Lambda}(k_{pp}^*; R) = \sum_{k_{p\Lambda}^*} C_{p\Lambda}(k_{p\Lambda}^*) T(k_{pp}^*, k_{p\Lambda}^*)$ - theoretical p Λ correlation function for given R obtained
- 185 from Lednický's model,
- 186 – $T(k_{pp}^*, k_{p\Lambda}^*)$ - transformation factors related to Λ decay kinematics, calculated with THERMINATOR.

187 The p Λ correlation function obtained with Lednický's model is calculated as a function of $k_{p\Lambda}^*$, but
 188 according to Eq. (2), there is a need to use $C_{p\Lambda}$ dependent on the relative momentum between two
 189 protons. Therefore, relevant transformation should be performed, namely for each value of k_{pp}^* , $C_{p\Lambda}$ is
 190 determined as a sum over all $k_{p\Lambda}^*$ values of $C_{p\Lambda}$ obtained with Lednický's model scaled by factors from
 191 the two-dimensional histogram $T(k_{pp}^*, k_{p\Lambda}^*)$ calculated with THERMINATOR:

$$C_{p\Lambda}(k_{pp}^*; R) = \sum_{k_{p\Lambda}^*} C_{p\Lambda}(k_{p\Lambda}^*) T(k_{pp}^*, k_{p\Lambda}^*). \quad (3)$$

192 The kinematics dependence of Λ decay $T(k_{pp}^*, k_{p\Lambda}^*)$ is shown in Fig. 13. Fig. 14 shows an example of the
 193 transformation of $C_{p\Lambda}$.

As far as fitting the p \bar{p} correlations are concerned, the relevant formula is analogous to Eq. (2) and takes the following form:

$$C_{\text{meas}}(k_{p\bar{p}}^*) = 1 + \lambda_{pp} \cdot (C_{pp}(k_{pp}^*; R) - 1) + \lambda_{p\Lambda} \cdot (C_{p\Lambda}(k_{pp}^*; R) - 1). \quad (4)$$

194 The p \bar{p} correlation function calculated with the analytical model of Lednický and Lyuboshitz and its
 195 form after the transformation to the reference frame of two protons (one of which comes from Λ decay)
 196 are shown in Fig. 15.

197 pp (p \bar{p}) and p Λ (p $\bar{\Lambda}$) correlation functions have been calculated for the emission radii from 1.0 fm to
 198 6.0 fm with a step of 0.1 fm. The fitting procedure is performed making use of MINUIT minimisation
 199 package. A gradient minimisation algorithm (MIGRAD) is used to find a minimum χ^2 value calculated

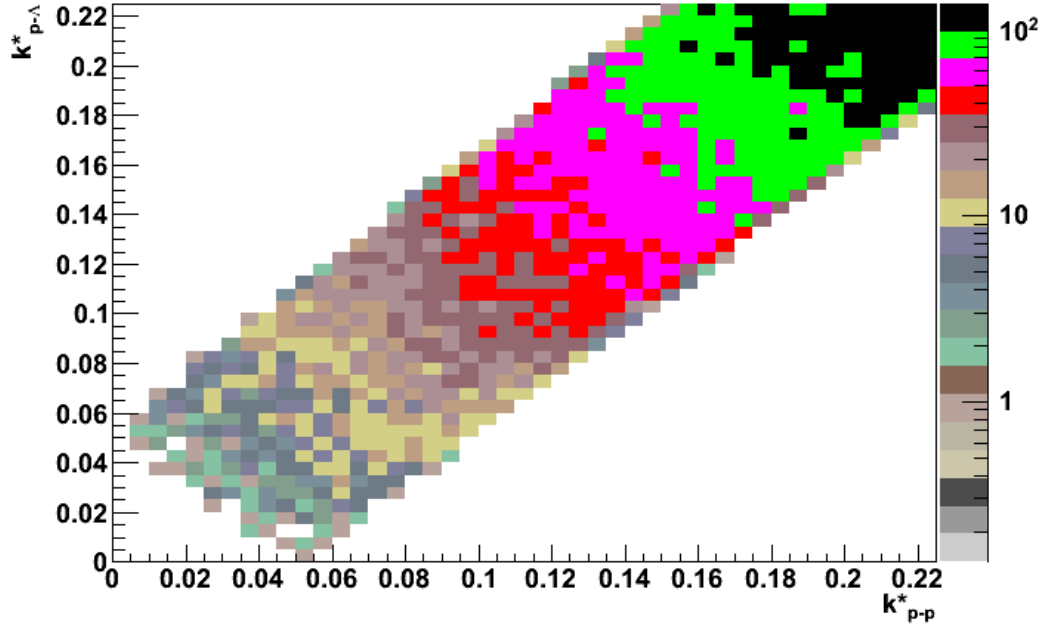


Fig. 13: Kinematics dependence of Λ decay $T(k_{pp}^*, k_{p\Lambda}^*)$ calculated with THERMINATOR.

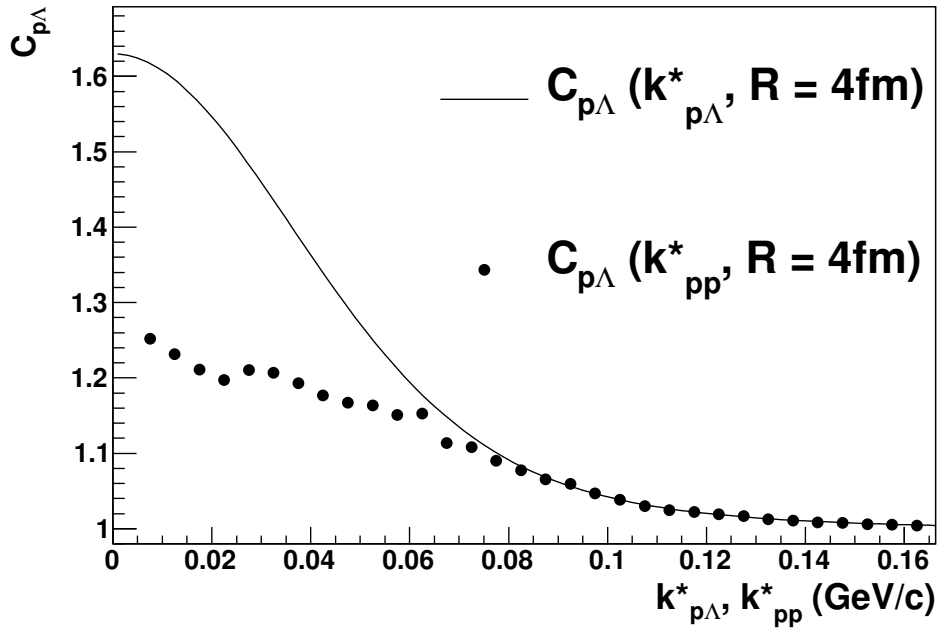


Fig. 14: Example of the transformation of $C_{p\Lambda}(k_{p\Lambda}^*) \rightarrow C_{p\Lambda}(k_{pp}^*)$.

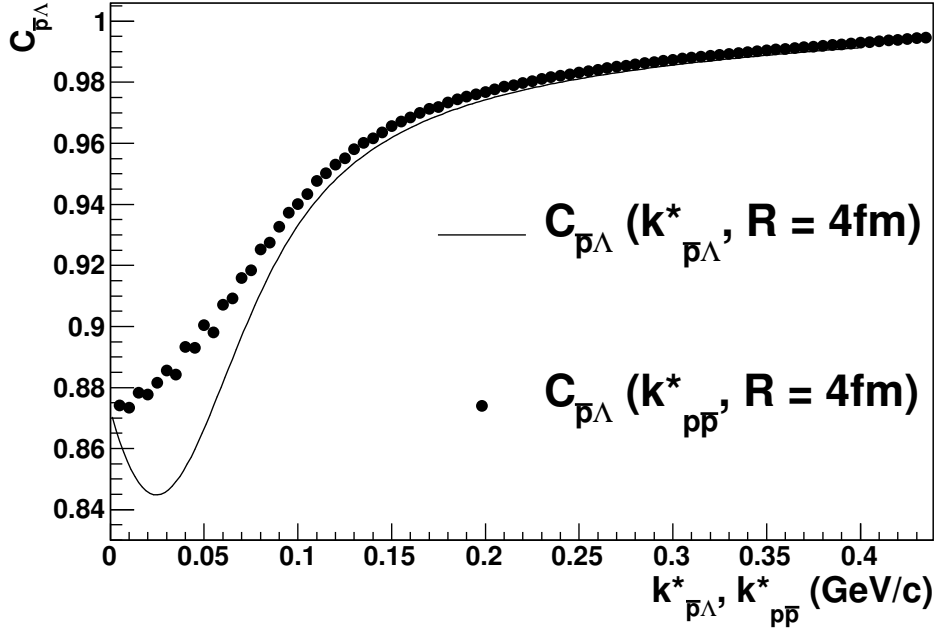


Fig. 15: The $\bar{p}\Lambda$ correlation function calculated with the analytical model of Lednicky and Lyuboshitz and its form after the transformation: $C_{\bar{p}\Lambda}(k_{\bar{p}\Lambda}^*) \rightarrow C_{\bar{p}\Lambda}(k_{p\bar{p}}^*)$.

between the experimental correlation function and the functions defined by Eq. (2) and (4) calculated for given parameters λ_{pp} , $\lambda_{p\Lambda}$ ($\lambda_{p\bar{p}}$, $\lambda_{\bar{p}\Lambda}$) and R by the quadratic interpolation of the theoretical correlation functions. It is assumed that the radii of pp ($p\bar{p}$) and $p\Lambda$ ($\bar{p}\Lambda$) sources are equal.

Fig. 16 and 17 are the examples of the fitting results for $\bar{p}\bar{p}$ and $p\bar{p}$ correlation functions. The fit qualitatively works, namely contribution from pp correlations describes the maximum at $k^* \approx 20$ MeV/c and wide correlations is reproduced by residual correlations coming from $p\Lambda$ system.

We found following sources of the systematic errors:

- constraints on the λ_{pp} , $\lambda_{p\Lambda}$ parameters
 - fixing the ratio $\lambda_{pp}/\lambda_{p\Lambda}$ to values estimated from the fits to pp , $\bar{p}\bar{p}$, $p\bar{p}$, setting the λ_{pp} and $\lambda_{p\Lambda}$ parameters free, causes the maximum change of the radius 13% (usually $< 5\%$)
 - fixing to estimates from AMPT (see Tab.1): in general, fit fails, hence it is not considered in the systematics error,
- fitting procedure
 - ranges of the fit and starting parameters - changing the fit range by $\pm 10\%$ causes the maximum change less than 6% for the radius (usually $< 2\%$); the fit is quite sensitive to significant changes of the starting parameters, but close to the minimum of the objective function, the change of the radius is negligible (however it is still under investigation)
 - stability of the numerical fit - $< 10\%$ (usually $< 3\%$)
- assumption regarding $R_{p\Lambda}/R_{pp}$ ratio (following m_T scaling from hydrodynamics) - taking $R_{p\Lambda} = 0.95R_{pp}$ causes the change of the radius less than 1%
- influence of the two track cuts (turning on and off the ϕ^* cut) - $< 10\%$ (usually $< 4\%$)

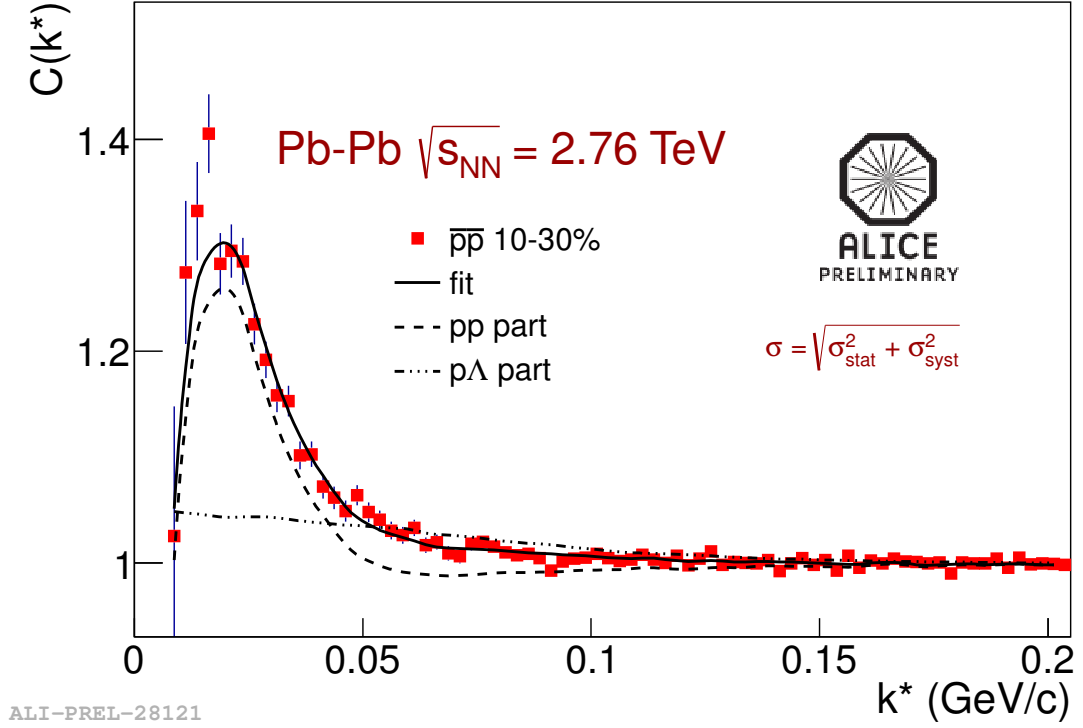


Fig. 16: Results of the fitting the $\bar{p}p$ correlation function. The contribution of the theoretical pp and p Λ correlation functions scaled by factors related to the relevant fractions of pp pairs are shown with dashed and dotted-dashed lines, respectively.

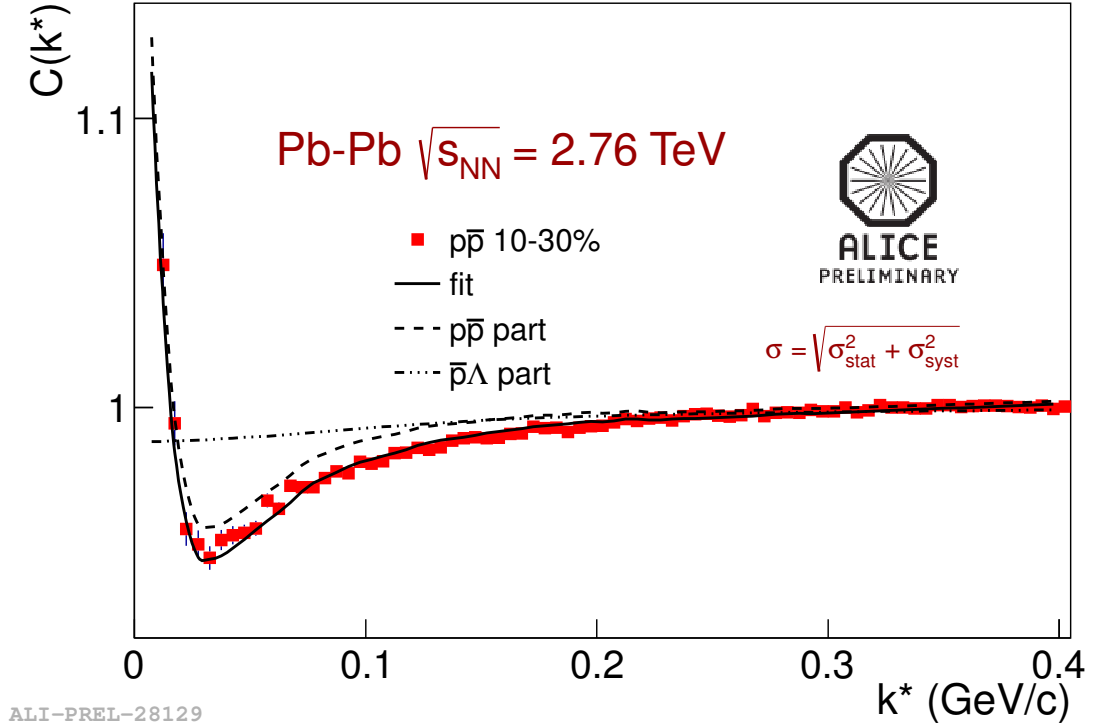
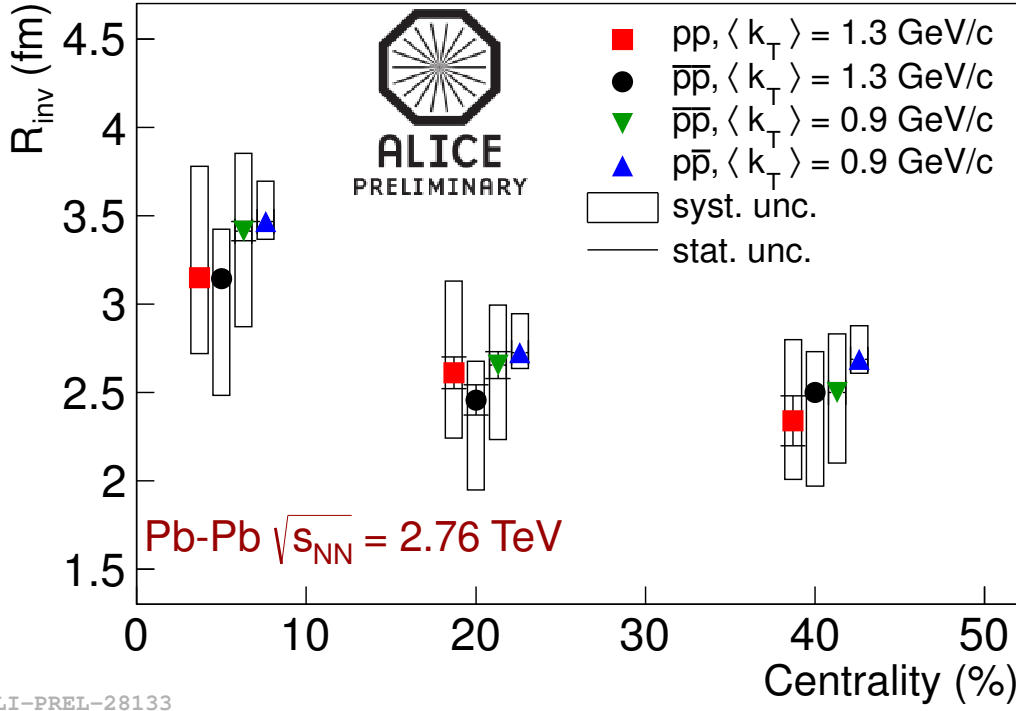


Fig. 17: Results of the fitting the $p\bar{p}$ correlation function. The contributions of the theoretical $p\bar{p}$ and $p\bar{\Lambda}$ correlation functions scaled by factors related to the relevant fractions of $p\bar{p}$ pairs are shown with dashed and dotted-dashed lines, respectively.



ALI-PREL-28133

Fig. 18: Centrality dependence of the fitted radii from proton femtoscopy. Statistical (lines) and systematic (boxes) errors are shown.

Systematic error for given system, centrality and k_T bin is estimated as the maximum error within each system. Maximum systematic error for the radius is estimated as: +20%, -21%.

Tab. 2 contains the numerical values of the fitted radii with statistical and systematic errors. Fig. 18 shows the monotonic centrality dependence of the fitted radii for all combinations of pairs of (anti)protons.

| $\langle k_T \rangle$ (GeV/c) | R (fm) | | | |
|-------------------------------|---------------------------------|---------------------------------|---------------------------------|---------------------------------|
| | pp | $\bar{p} \bar{p}$ | | $p \bar{p}$ |
| | 1.3 | 0.9 | 1.3 | 0.9 |
| 0-10% | $3.15 \pm 0.05^{+0.63}_{-0.43}$ | $3.41 \pm 0.05^{+0.44}_{-0.54}$ | $3.14 \pm 0.04^{+0.28}_{-0.66}$ | $3.47 \pm 0.05^{+0.23}_{-0.10}$ |
| 10-30% | $2.61 \pm 0.09^{+0.52}_{-0.37}$ | $2.65 \pm 0.08^{+0.34}_{-0.42}$ | $2.45 \pm 0.09^{+0.22}_{-0.51}$ | $2.73 \pm 0.02^{+0.19}_{-0.08}$ |
| 30-50% | $2.34 \pm 0.14^{+0.46}_{-0.33}$ | $2.50 \pm 0.01^{+0.33}_{-0.40}$ | $2.50 \pm 0.01^{+0.23}_{-0.53}$ | $2.69 \pm 0.02^{+0.19}_{-0.08}$ |

Table 2: Radii extracted from proton femtoscopy. Statistical and systematic errors are shown.

In Fig. 19 radii obtained in proton femtoscopy as well as those extracted from $\pi\pi$, $K^\pm K^\pm$ and $K_S^0 K_S^0$ correlations are plotted versus $m_T = \sqrt{\langle k_T \rangle^2 + m_0^2}$. R_{inv} is scaled by the approximate kinematic factor $(\frac{\sqrt{\gamma}+2}{3})^{-1/2}$. Hydrodynamics predicts m_T of the radii calculated in LCMS (Longitudinally Co-Moving System). However, R_{inv} is calculated in PRF (Pair Rest Frame). Therefore, approximate m_T scaling may be recovered by using the given formula. In Fig. 20 results for charged and neutral kaons as well as for (anti)protons are combined using weighted mean method:

$$R_{\text{mean}} = \frac{\sum_i R_i w_i}{\sum_i w_i}$$

$$SystErr_{\text{mean}} = \frac{\sum_i SystErr_i w_i}{\sum_i w_i} + diff$$

$$w_i = \frac{1}{\sigma_i^2}$$

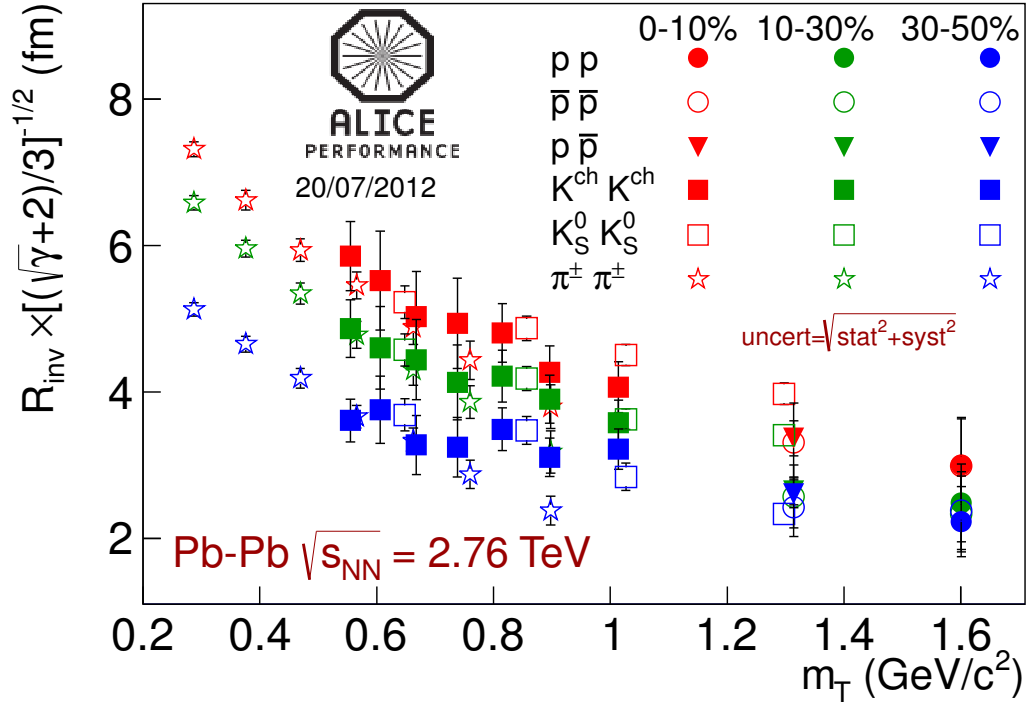


Fig. 19: m_T dependence of the radius parameter extracted from correlations of pions, charged kaons, neutral kaons and protons. Estimates of total errors (the quadrature sum of the statistical and the systematic ones) are shown.

where σ_i - statistical error, *diff* - the difference in radius between different pair types. Results for kaons are combined in the following way:

- 1.-4. m_T bins $K^{ch}K^{ch}$ + 1. m_T bin $K_S^0K_S^0$
- 5.-6. m_T bins $K^{ch}K^{ch}$ + 2. m_T bin $K_S^0K_S^0$
- 7. m_T bin $K^{ch}K^{ch}$ + 3. m_T bin $K_S^0K_S^0$
- 4. m_T bin $K_S^0K_S^0$

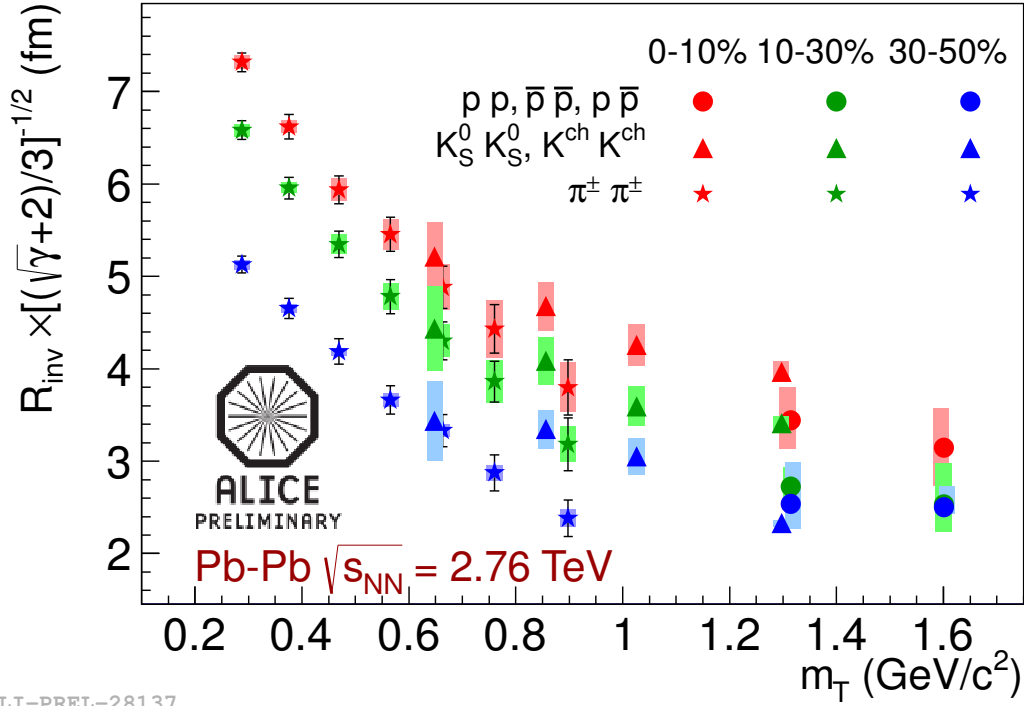
For protons, we combined the first m_T bins for $p\bar{p}$ and $\bar{p}\bar{p}$ and the second m_T bins for pp and $p\bar{p}$.

4 Summary

In summary, correlations of all combinations of pairs of protons and antiprotons have been measured in Pb-Pb collisions at $\sqrt{s_{NN}} = 2.76$ TeV in the ALICE experiment. The femtoscopic parameters for the radius of the proton source are extracted from one-dimensional pp , $\bar{p}\bar{p}$ and $p\bar{p}$ correlation functions. The fit includes final-state interactions and quantum statistics for identical pairs of (anti)protons. The fit takes into account residual correlations coming from pA system. Two-proton correlations show an increase of the radius with increasing multiplicity and slight decrease of the radius with increasing pair transverse momentum.

References

- [1] The ALICE Collaboration: *Two-pion Bose-Einstein correlations in central PbPb collisions at $\sqrt{s_{NN}} = 2.76$ TeV*; Phys.Lett.B696:328-337,2011



ALI-PREL-28137

Fig. 20: m_T dependence of the radius parameter extracted from correlations of pions, charged kaons, neutral kaons and protons. Results for charged and neutral kaons as well as for (anti)protons are combined using weighted mean method (see text for details).

- [2] Gos, H. P. for the STAR collaboration : *Proton - proton, anti-proton - anti-proton, proton - anti-proton correlations in Au+Au collisions measured by STAR at RHIC*; Eur.Phys.J. C49 (2007) 75-80
- [3] Kisiel, A., Taluc, T., Broniowski W., Florkowski, W.; *THERMINATOR: THERMal heavy-IoN generatorATOR*; Comput.Phys.Commun. 174 (2006) 669-687
- [4] Kisiel, A.: *CorrFit - a program to fit arbitrary correlation functions*; Nukleonika 49;Suppl 2:s81-s83 (2004)
- [5] Lednicky, R.: *Finite-size effects on two-particle production in continuous and discrete spectrum*; Phys.Part.Nucl. 40 (2009) 307-352
- [6] The LHC Computing Grid software development portal Savannah: https://savannah.cern.ch/bugs/?func=detailitem&item_id=75267
- [7] Christian Klein-Boesing, private communication
- [8] Malinina, L.: <https://indico.cern.ch/getFile.py/access?contribId=22&sessionId=6&resId=0&materialId=slides&confId=147108>
- [9] Gramling, J.L. <http://indico.cern.ch/getFile.py/access?contribId=42&sessionId=16&resId=0&materialId=slides&confId=146554>